A metapopulations epidemic model and its measures for potential mitigation

Un modelo epidémico de metapoblaciones y sus medidas para su posible mitigación

Tomas Veloz[1,2,3]

[1] *Fundación para el Desarrollo Interdisciplinario de la Ciencia, la Tecnología y las Artes - DICTA, Santiago, Chile*
[2] *Centre Leo Apostel for Interdisciplinary Studies, Vrije Universiteit Brussel, Belgium*
[3] *Universidad Andres Bello, Facultad de Ciencias para la Vida, 8370146 Santiago, Chile*

Reception date of the manuscript: 01/03/2022
Acceptance date of the manuscript: 01/04/2022
Publication date: 29/04/2022

Abstract—Strategies attempting to reduce the impact of Covid19 attempted harnessing available geo-spatial, demographic, and behavioural data. Such data has shown to be extremely useful for identifying drivers behind the transmission of the disease. In this article, we develop a toy model emulating the spatial and demographic features of Santiago de Chile, quantify the presence and interaction among different groups in the different spaces defined by the model, and show that effects of the infection dynamics are hidden in the infection data that is usually fitted. In partiucular, we show that the distribution of contagion rates among different sectors distributes as a power-law regardless of the pandemic situation (outbreak vs full spread), and that the power-law distribution strongly depends on a social segregation.

Keywords—Biomathematics, Mathematical Biology, Mathematical Ecology, Mathematical Epidemiology, Mathematical Biotechnology

Resumen— Las estrategias que intentan reducir el impacto de Covid19 intentaron aprovechar los datos geoespaciales, demográficos y de comportamiento disponibles. Dichos datos han demostrado ser extremadamente útiles para identificar las razones detrás de la transmisión de la enfermedad. En este artículo, desarrollamos un modelo de juguete que emula las características espaciales y demográficas de Santiago de Chile, cuantificamos la presencia e interacción entre diferentes grupos en los diferentes espacios definidos por el modelo y mostramos que hay efectos espaciales de la dinámica de infección que están ocultos en las tasas de infección que se ajustan desde los datos. En particular, mostramos que la distribución de las tasas de contagio entre diferentes sectores se distribuye como una ley de potencia independientemente de la situación de pandemia (brote vs propagación total), y que la distribución de la ley de potencia depende fuertemente de un parametro que mide la segregacion social.

Palabras clave— Biomatemática, Biología Matemática, Ecología Matemática, Epidemiología Matemática, Biotecnología Matemática

Introduction

Ihyroid Identifying strategies to control the spread of Covid19 or future epidemics is a major challenge in mathematical biology. On the one hand it is necessary to optimize not only the prevention of new cases but also the well-being of people. On the other hand, strategies must be feasible from a logistic and political perspective. Hence, generating models that allow estimating the dynamics of an epidemic is an urgent endeavour in our new context of global pandemics (PhD et al., 2020; Haug et al., 2020; Prem et al., 2020; Gozzi et al., 2021).

Meta-population models (Calvetti et al., 2020) are specially suited to meet the abovementioned challenge. Namely, these models are able to consider multiple interaction sectors and establish different dynamics within them. These interaction sectors are not restricted to be defined by spatial conditions only. They can incorporate other sources of information that are relevant to specify how interactions occur. Examples of these can be whether the place is a restaurant or a park, whether the interaction sector is restricted to certain population conditions, (school, hospital, or areas that can only be reached by car), and determine different infection rates and types of interaction depending on the behavioural patterns

of people within and across sectors over time (Shinde et al., 2020; Lauer et al., 2020; Eubank et al., 2020; Chang et al., 2021; Gozzi et al., 2021).

As an example of our approach, we develop a metapopulation model based on the SEIR model inspired in the case of Santiago, Chile, assuming $n = 5$ spatial sectors which aggregate groups of sectors of different income, and the non-homogeneous inter-sector mobility of the city, and study the distribution of rates of infection corresponding to different kinds of interaction. Namely, for an interaction to take place we define three spatial sector indexes: one corresponding to the address of the susceptible individual, another corresponding to the address of the infected individual, and another corresponding to the location at which the interaction takes place. Therefore, the rate of interaction is a 3-dimensional tensor, so-called impact tensor.

Interestingly, we show that the distribution of infection rates of the impact tensor distribute as a power law irrespective of the pandemic situation (outbreak or spread infection), and explore the influence of a sociual segregation parameter which modulates how likely is to have an interaction among different social (inmcome) groups. This work is of exploratory nature, after showing the model and our numerical results we present a discussion with possible ways to extend this work.

A METAPOPULATIONS EPIDEMIC MODEL

The SEIR model

In order to introduce the reader to the epidemiologic modelling we will introduce the most common epidemiologic model, which does not consider metapopulations, but a collection of people interacting in a single sector by means of a deterministic Susceptible-Exposed-Infected-Recovered (SEIR) compartmental model (Li and Muldowney, 1995) (see Fig. 1). Susceptible individuals experience an incubation period (the 'exposed' state), such that the individual is infected but not yet infectious for a significant period of time.

Fig. 1 shows how individuals transit through the compartments representing different epidemic states in the model.

The parameter β corresponds to the probability of transmission of the disease given an interaction between a susceptible and an infectious individual. The incubation rate, σ, is the rate of latent individuals becoming infectious (average duration of incubation is $\frac{1}{\sigma}$). Recovery rate, $\gamma = \frac{1}{D}$, is determined by the average duration, D, of infection.

The equations that rule the evolution of the system are deduced from the following assumptions:

- β depends on the virus type only and thus is constant.
- The rate of interaction events for a susceptible individual is proportional to the density of infected people in the sector, given by $\frac{I}{N}$.

The equations of the SEIR model are thus

$$\begin{aligned} \dot{S} &= -\beta \frac{SI}{N} \\ \dot{E} &= \beta \frac{SI}{N} - \sigma E \\ \dot{I} &= \sigma E - \gamma I \\ \dot{R} &= \gamma I \end{aligned} \tag{1}$$

This infection dynamics of eq. (1) is a coarse approximation of a realistic epidemic situation because it assumes random mixing of people, and that the success rate of infection is independent. One common way to overcome this unrealistic assumption is to define a saturated infection rate Sun and Min (2014)

$$\dot{S} = -\beta \frac{SI}{1 + \alpha I} \tag{2}$$

where α is a parameter which measures the maximum amount of infection events that can occur per time unit. However, saturation rate might depend on factors that modulate the way people interact with each other such as age, behavioral attitudes, and time and space dependency of the population density (Takeuchi et al., 2000; Rohith and Devika, 2020; Kumar et al., 2020). We will thus make use of a metapopulations model in order to incorporate the latter aspect in this paper.

Metapopulations and effective populations

In a metapopulation model, we start from a population N inhabiting different sectors $i = 1, ..., n$. For simplicity we assume no birth occurs. For each sector $i = 1, ..., n$, we define $S_i(t), E_i(t), I_i(t), R_i(t)$ as the amount of susceptible, exposed, infected and recovered inhabitants of sector i, respectively, at time t. Note that $S_i(t) + E_i(t) + I_i(t) + R_i(t) = N_i(t)$ is constant, and $\sum_{i=1}^{n} N_i(t) = N$.

Since inhabitants of each sector can move to other sectors for their daily activities, we assume that a proportion $P_{ij}(t)$ of population from sector i is in sector j at time t. Clearly, $P_{ii}(t)$ corresponds to the proportion of inhabitants that stay at their own sector at time t. $P_{ij}(t)$ is called *mobility matrix*.

Since the rate of infection in the SEIR model is proportional to the density of infected individuals in a sector, and $P_{ij}(t)$ implies a change of suchg density over time, we need to obtain the *effective populations* of the different epidemic states at each sector. The total effective population of each sector i, denoted by $\bar{N}_i(t)$, corresponds to the total population of sector i minus its outflow to other sectors plus the inflow of populations from other sectors. Hence:

$$\begin{aligned} \bar{N}_i &= N_i - \sum_{j \neq i} P_{ij}(t) N_i + \sum_{j \neq i} P_{ji}(t) N_j \\ &= N_i - \left(\sum_{j=1}^{n} P_{ij}(t) N_i - P_{ji}(t) N_j \right) \end{aligned} \tag{3}$$

Note that in the right hand side of (3), the term $P_{ii}(t)N_i$ is added and subtracted, helping to simplify the presentation of the formula. However, it is possible to rewrite Eq. (3) in a simpler way by counting only those staying at sector i plus

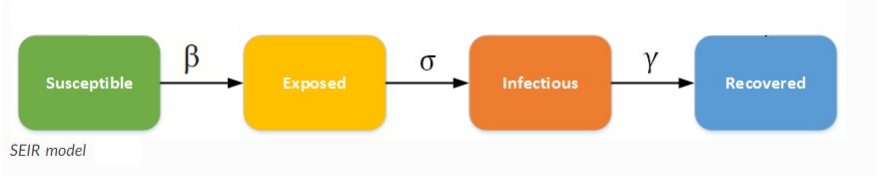

Figure 1: SEIR compartmental model.

the inflow from other sectors:

$$\bar{N}_i = N_i P_{ii}(t) + \sum_{j\neq i} N_j P_{ji}(t) = \sum_{j=1}^{n} N_j P_{ji}(t) \tag{4}$$

Similarly, the infected effective population of sector i is given by

$$\bar{I}_i = \sum_{j=1}^{n} I_j P_{ji}(t), \tag{5}$$

ssible ways in which incoming and outgoing groups can interact.

Mobility and demographics driven infection rates

In order to calculate the rate of infections in our metapopulation model, we must take into consideration that the infection event in formula (1) involves three entities that are now indexed by a sector coordinate. Namely, one coordinate denotes the sector associated to the susceptible individual, another coordinate denotes the sector of the infected individual, and another coordinate denotes the sector at which the interaction takes place. Hence, consider a sector k at time t, and let's estimate the rate p_{ijk} of interactions between the susceptible population from sector i (given by $P_{ik}(t)S_i(t)$) and the infected population from sector j (given by $P_{jk}I_j(t)$), out of a total of people in sector k (given by $\bar{N}_k$). In order to make our model reasonable with respect to mobility and for incorporating an example of how demographics changes the interactions we assume the following:

- Inhabitants of each sector $i = 1,...,n$ can be at home or not at home, and a parameter $0 \leq \lambda_i(t) \leq 1$ regulates the proportion of people from sector i at home during the course of a day.
- Mobility of people being not at home, from sector i to sector j is ruled by $P_{ij}(t)$.
- Each sector is associated to an income group which can be Low, Middle, or High, and there is function $g_{ij}(s)$ which weights the relative amount of interactions between the different groups given by

$$g_{ij}(s) = \begin{cases} 1 \text{ if } i \text{ and } j \text{ are of same income group} \\ s, \text{ if } i \text{ and } j \text{ are of neighboring income groups} \\ s^2, \text{ if } i \text{ and } j \text{ are of distant income groups} \end{cases} \tag{6}$$

- Interactions at home are ruled by a saturated dynamics (see eq. 2) with saturation parameter α, while interactions not at home are ruled by a mass-action dynamics (see eq. (1)).

Following these assumptions, we specify $p_{ijk}(t)$ in consistency with the assumptions as follows

$$p_{ijk}(t) = \begin{cases} \beta S_i(t) I_i(t) P_{ii}^2(t) \left(\frac{\lambda_i^2(t)}{1+\alpha I_i(t)} + \frac{(1-\lambda_i(t))^2}{\bar{N}_i(t)} \right), \text{ if } i = j = k \\ \beta g_{ij}(s) S_i(t) I_j(t) P_{ik}(t) P_{jk}(t) \frac{(1-\lambda_i(t))(1-\lambda_j(t))}{\bar{N}_k(t)}, \text{else} \end{cases} \tag{7}$$

Note that $p_{ijk}(t)$ depends on the choice of parameters α, and s, and the shape of $\lambda_i(t)$ and $g_{ij}(s)$. Different choices of these parameters correspond to different modeling situations. In order to obtain the contagion rate per sector, note that

$$\sum_{j,k=1}^{n} p_{ijk}(t) \tag{8}$$

indicates all the possible ways in which susceptible individuals from sector i can get infected. Therefore, the SEIR system of equations (1) can be easily extended to its metapopulation version as follows:

$$\begin{aligned} \frac{dS_i}{dt} &= -\sum_{j,k=1}^{n} p_{ijk}(t) \\ \frac{dE_i}{dt} &= \sum_{j,k=1}^{n} p_{ijk}(t) - \sigma E_i \\ \frac{dI_i}{dt} &= \sigma E_i - \gamma I_i \\ \frac{dR_i}{dt} &= \gamma I_i \end{aligned} \tag{9}$$

This model is equivalent to the SEIR model for the incubation and recovery dynamics, but since the contagion dynamics is modified by the fact that the infection event can occur in different sectors, and those events depend on the mobility, occupation of spaces and social differences, we call it 'SEIR*'. Note that the solution of the SEIR* model delivers the number of individuals at each epidemic-state at each sector over time. Since population data, infection data collected by authorities, demogaphic and mobility data collected by phone companies is associated to each person's home address, the SEIR* model is compatible with high spatial resolution data.

AN EXAMPLE OF SEIR* BASED ON SANTIAGO DE CHILE

The following example is inspired in the population and mobility structure of Santiago, Chile. We will use this example to illustrate the SEIR* model and the features of the impact tensor.

City structure and Population

Our model of Santiago corresponds to a division of its counties (comunas) into five sectors representing clusters having similar mobility and social-interaction-pattern structures. Our model of Santiago is composed by a central downtown sector ($i = 2$) surrounded by east ($i = 0$), north ($i = 1$), west ($i = 3$) and south ($i = 4$) sectors, such that the west, north, and south sectors, contain a large population having middle, low, and low income on average respectively, and that do not receive too many people from other sectors due to the lack of jobs and places of interest. Those populations tend to mobilize to the other two sectors for work and shopping. Those other two sectors, east and central, with high and medium income on average respectively, accumulate the majority of work places and concentrate the tourism and places of interest in general. Thus, the populations of these two sectors either move between each other or stay at their own sector. In addition, social-interactions are less frequent across groups of less similar average income.

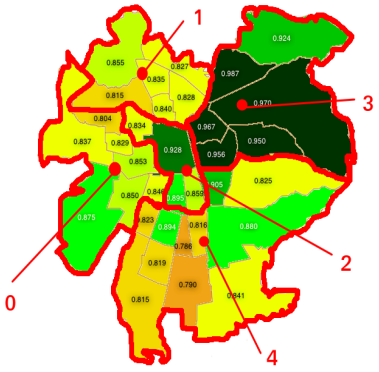

Figure 2: Sectorial division of Santiago, Chile. Color indicates a sociological variable that is correlated with average income of the sub-sector, where dark green indicates highest income and orange indicates lowest income.

Therefore, we have that

$$g_{ij}(s) = \begin{pmatrix} 1 & 1 & s & s^2 & 1 \\ 1 & 1 & s & s^2 & s \\ s & s & 1 & s & s \\ 1 & 1 & s & s^2 & 1 \\ 1 & 1 & s & s^2 & 1 \end{pmatrix}. \tag{10}$$

The *segregation parameter* s helps to differentiate social structures with low segregation, i.e. where high and low income people occupy the same spaces, and thus interaction patterns do not depend on income (case $s \sim 1$), and social structures with high segregation, i.e. where high and low income people do not encounter in the same spaces, and thus interaction patterns strongly depend on income (case $s \sim 0$).

sector	N_i	Mobility tendency	ave. income
0	1.5M	$\{2,3,1,4\}$	Low
1	1.3M	$\{2,3,0,4\}$	Low
2	0.7M	$\{3,[0,1,4]\}$	Middle
3	1.1	$\{2,[0,1,4]\}$	High
4	1.8	$\{2,3,[0,1]\}$	Low

Figure 3: Description of our mobility and social income model. First column indicates sector, second column indicates population, third column indicates mobility preference (sectors in brackets there is equal preference), fourth column indicates average income.

Inter-sector daily mobility model

Inter-sector mobility changes over the course of the day. Thus, we will assume that mobility increases linearly from 4am to 16pm, and decreases linearly between 16pm to 4am, reaching not mobility at 4am.

For simplicity, we will re-scale time, so the hours of the day run cyclically between 0 and 1, with 4am corresponding to 0 and 16pm corresponding to $\frac{1}{2}$.

Hence, the proportion of people moving from sector i to sector j at time t is given by $P_{ij}(t)$ with $0 \leq t \leq 1$, with

$$P_{ij}(0) = \begin{pmatrix} 1 & 0 & 0 & 0 & 0 \\ 0 & 1 & 0 & 0 & 0 \\ 0 & 0 & 1 & 0 & 0 \\ 0 & 0 & 0 & 1 & 0 \\ 0 & 0 & 0 & 0 & 1 \end{pmatrix} = \mathbf{1}, \tag{11}$$

when no mobility is happening, i.e. everyone at home, and

$$P_{ij}\left(\frac{1}{2}\right) = \begin{pmatrix} 0{,}4 & 0{,}1 & 0{,}25 & 0{,}2 & 0{,}05 \\ 0{,}1 & 0{,}4 & 0{,}25 & 0{,}2 & 0{,}05 \\ 0{,}1 & 0{,}1 & 0{,}5 & 0{,}2 & 0{,}1 \\ 0{,}05 & 0{,}05 & 0{,}2 & 0{,}65 & 0{,}05 \\ 0{,}05 & 0{,}05 & 0{,}25 & 0{,}25 & 0{,}4 \end{pmatrix}, \tag{12}$$

For the peak mobility moment of the day at 16pm. Since the change of mobility for $0 \leq t \leq \frac{1}{2}$ increases linearly, and decreases symmetrically between $\frac{1}{2} \leq t \leq 1$, we have that in general

$$\begin{aligned} P_{ij}(t) &= P_{ij}(0) - h(t)\left(P_{ij}(0) - P_{ij}\left(\frac{1}{2}\right)\right), \text{ with} \\ h(t) &= \begin{cases} 2t \text{ if } 0 \leq t \leq \frac{1}{2} \\ 2-2t, \text{ if } \frac{1}{2} \leq t \leq 1 \end{cases} \end{aligned} \tag{13}$$

Effective populations

The effective populations defined by (3) evolve during the day as shown in figure 4

Note that in fig. 4 sectors $k = 2$ and $k = 3$ have a high positive variation in their effective populations while other sectors have a negative variation. Indeed, population in sectors $k = 2$ and $k = 3$ increase nearly 2.5 and 1.5 times respectively, while the decrease of population in other sectors ranges between 0.6 and 0.7.

Another interesting phenomena that can be observed in fig. 4 is that the effective populations of sectors 2 and 3 become larger than the effective population of other sectors at different times. For example, $\bar{N}_3 > \bar{N}_1$ around 6am, and $\bar{N}_3 > \bar{N}_4$ around 9am, and due to our symmetric assumptions this is reversed at 2am and 23pm respectively. The latter implies that not only the effective population radically changes over time, but also that there are certain moments at which the effective population changes structurally, i.e. the ordering of sectors in terms of effective population changes.

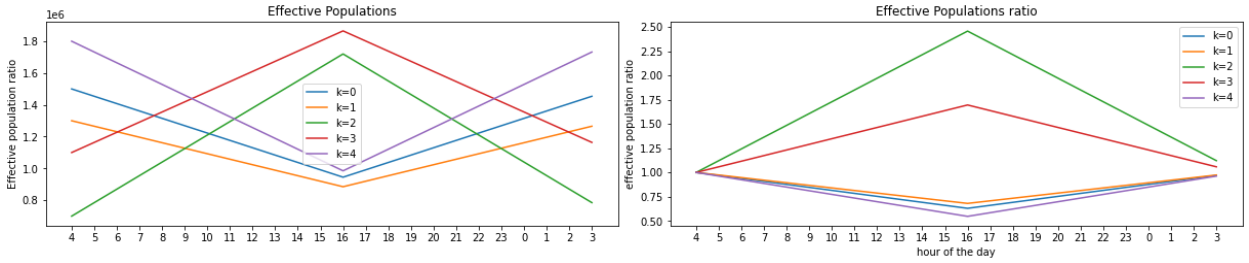

Figure 4: Population structure over the course of one day. Left:Effective populations. Right: Ratio between effective and total population. Colors $k = 1, \ldots, 5$.

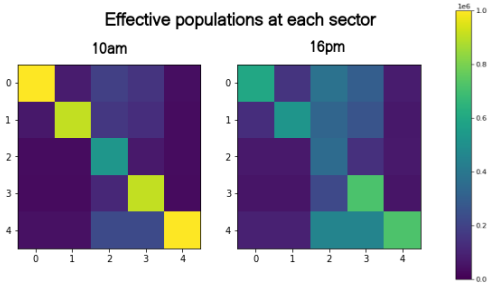

Figure 5: Effective populations from each sector at each sector. Left: 10am. Right: 16pm (peak mobility time).

In figure 5 we can observe the effective population from each sector at each other sector, i.e. the matrix $P_{ij}(t)N_i$ at two different times of the day. The assumption that sectors 0, 1, and 4 do not receive several people from other sectors, as well as the fact that sectors 2 and 3 have a more homogeneous population structure (specially 2), can be clearly seen in the right subfigure.

A first look on the distribution of infection rates

Since we observe that mobility induces major changes in the effective populations, we are interested in seeing the way in which the infection rates distribute in different circumstances. As a first attempt to understand such distributions, we will illustrate the difference of the distribution of rates at the moment of highest mobility (16pm) in two pandemic situations. The first situation corresponds to an outbreak in sector 3 (as it happened in reality), and we represent it by having 120 infected individuals in sector 3, and only 20 infected individuals in each of the other sectors. The second situation emulates dispersion of the epidemy, and is represented by having 1 % of the population infected in all sectors equally.

In fig. 6 we plot the distribution of rates of both situations choosing $s = 1$. There are various interesting aspects to mention about the plots. Before doing so we must mention that in order to obtain a 2D plot of an object which depends on 3 spatial indexes, we defined the following (bijective) function to represent the triplets representing the rate p_{ijk}

$$d(i, j, k) = (i + 5j + 25k) \tag{14}$$

The function d generates an index ranging from 0 to 124 to represent all possible combinations of triplets $\{i, j, k\}$ with $i = 0, \ldots, 4$. Hence, we do not have a direct view on the sector triplets where the distribution peaks. Thus, we will focus on general properties of the distribution rather in the values for specific triplets.

Regarding the shape of the distribution, first notice that in both the outbreak and dispersed situation the majority of triplets $\{i, j, k\}$ have a small associated rate, and only a few collections of triplets accumulate reach high values. This is an indication that the distribution of reaction rates might exhibit a power-law distribution. The latter is more clearly seen in the left orange curves. The power-law like distribution should not be unexpected for an outbreak situation, as most infected individuals are concentrated in a single sector and thus it is rare to encounter significant infection rates away from the interaction zone of sector 3. However, for the dispersed case we obtain a very similar distribution pattern, although the peaks can be seen to be different from those at the outbreak. This is a rather unexpected result because simple reasoning would indicate that in the situation of dispersion the infection rates should tend to homogeneize. However, we still see a strong accumulation in only some triplets. In order to better comprehend this aspect we take look to the right plots in fig. 6 which show the sorted (from larger to smaller) infection rates in log-scale. We observe that a linear curve provides a good approximation to the log-data, and that although the distribution in the dispersion case is fitted with a smaller slope than in the outbreak situation (which indicates that infection rates are more homogeneous in the case of dispersion), still the linear fit provides a good approximation. It is indeed of special interest the fact that in both cases the triplets with highest contagion rates (at the left of the curve) follow a different slope than the rest of the curve. We could perhaps provide a much better approximation of the data with a bi-modal linear approximation, one with higher slope in which all the high infection rate events concentrate, and another where the linear decay tendence is observed for the rest of the sectors.

In order to evidence the dependency of the results with the social segregation parameter, we rebuild these plots for the case $s = 0{,}4$ and plot them in fig. 7.

The case $s = 0{,}4$ in the case of the outbreak exhibits a completely different profile than in the case $s = 1$, which can be seen in the right top plot in fig. 7. Namely, the profile does not resembles a linear curve, but instead a tri-modal form, one first part with high slope and high values, then a middle flat zone, and finally a high slope with small values. This is coherent with the fact that the interaction patterns are very different for the three social groups. The case of epidemic dispersion looks again like a power-law distribution, but with a much higher slope than in the case $s = 1$. This indicates that

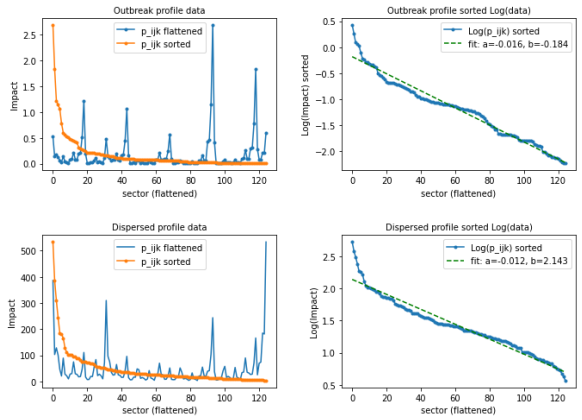

Figure 6: Distribution of infection rates when $s = 1$. Upper row corresponds to an outbreak situation, lower row corresponds to a situation of epidemic dispersion. The blue curves in the left plots display on the x−axis the triplet i, j, k by associating it to $d(i, j, k)$ defined in (14), and the y−axis shows the value p_{ijk} for the corresponding triplet. The orange curve shows how the distribution looks when sorted (irrespective of the indexes associated to the blue curve). The blue curve of the right plots show the log of the sorted rates, and the green curve shows the best linear fit of such sorted distribution as well as the values of slope (a) and intercept (b) that make such best fit.

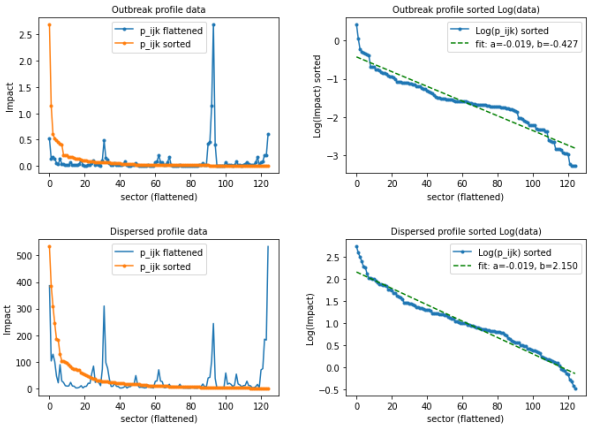

Figure 7: Distribution of infection rates when $s = 0{,}4$. Same description as in fig. 6

.

the sector triplets which are mostly responsible for the global contagion rates are much more highly concentrated in some specific interactions.

We conclude from this simple view that there seem to be a pattern of few specific triplets which regardless of the pandemic situation would have much higher kinetic rates than the large majority of other triplets. Therefore, mitigation strategies, i.e. interaction restrictions, could profit from this information to minimize the number of people participating in the mitigation strategy while maximizing the decrease of the infection rate. Moreover, the fact that in the case $s = 0{,}4$ we see that the slope approximating the log-curve of infection rates is higher than in the case $s = 1$, implies that efficient mitigation strategies could even be even more successful in the case of high social segregation.

Discussion

The results shown in this article open a large number of possible venues to explore First, the epidemic states and the features defining the individuals could be generalized. In this case we used the SEIR epidemic states, and applied only spatial and a social segregation parameter to identify populations. We could include age, sex, comorbilities, and several other demo demographic features, mobility profile, tendency to apply self-care measures, among others. Similarly, sectors could indicate sector use (grocery, store, park, restaurant, etc.). Therefore, we plan to extend our notation to incorporate these complexifications and thus represent the most advanced metapopulation models in a single framework (Fritz and Kauermann, 2020; Chang et al., 2021).

Second, we only worked out two pandemic situations but not the dynamical evolution of the system. This could be done by implementing the differential equations in a computational simulation, or by analytical studies.

Third, in case of trying to fit epidemic data we have that metapopulation models are multiparametric and non-linear, implying potentially strong sensitivity to parametric modifications, a change in parameters corresponding to a counterfactual measure, with respect to two parametric calibrations that fit equally good the known data, might lead to opposite conclusions. Therefore, it would be interesting to develop structural indicators, such as the slope of the sorted contagion rate curve (fig 7) or other aggregated indicators that might help to understand the dynamic of the pandemic.

We believe that explanatory mechanisms about the infection dynamics that take into consideration not only the epidemic time-series, but also the evolution of the multidimensional (geo-spatial, demographic, behavioural, etc.) structure of relevant events (infections, deaths, etc.) leading to the observed time-series shall be developed. We plan to do so in future work.

References

[1] Calvetti, D., Hoover, A. P., Rose, J., and Somersalo, E. (2020). "Metapopulation network models for understanding, predicting, and managing the coronavirus disease covid-19". *Frontiers in Physics*, 8:261.

[2] Chang, S., Pierson, E., Koh, P. W., Gerardin, J., Redbird, B., Grusky, D., and Leskovec, J. (2021). "Mobility network models of covid-19 explain inequities and inform reopening". *Nature*, 589(7840):82–87.

[3] Eubank, S., Eckstrand, I., Lewis, B., Venkatramanan, S., Marathe, M., and Barrett, C. L. (2020). "Commentary on ferguson, et al., impact of non-pharmaceutical interventions (npis) to reduce covid-19 mortality and healthcare demand". *Bull Math Biol*, 82(4):52.

[4] Fritz, C. and Kauermann, G. (2020). "On the interplay of regional mobility, social connectedness, and the spread of covid-19 in germany". *arXiv preprint arXiv:2008.03013*.

[5] Gozzi, N., Tizzoni, M., Chinazzi, M., Ferres, L., Vespignani, A., and Perra, N. (2021). "Estimating the effect of social inequalities on the mitigation of covid-19 across communities in santiago de chile". *Nature Communications*, 12(1):1–9.

[6] Haug, N., Geyrhofer, L., Londei, A., Dervic, E., Desvars-Larrive, A., Loreto, V., Pinior, B., Thurner, S., and Klimek, P. (2020). "Ranking the effectiveness of worldwide covid-19 government interventions". *Nature human behaviour*, 4(12):1303–1312.

[7] Kumar, A., Goel, K., et al. (2020). "A deterministic time-delayed sir epidemic model: mathematical modeling and analysis". *Theory in Biosciences*, 139(1):67–76.

[8] Lauer, S. A., Grantz, K. H., Bi, Q., Jones, F. K., Zheng, Q., Meredith, H. R., Azman, A. S., Reich, N. G., and Lessler, J. (2020). "The incubation period of coronavirus disease 2019 (covid-19) from publicly reported confirmed cases: Estimation and application". *Ann Intern Med*.

[9] Li, M. Y. and Muldowney, J. S. (1995). "Global stability for the seir model in epidemiology". *Mathematical biosciences*, 125(2):155–164.

[10] PhD, R. V., PhD, L. C. O., PhD, I. D., PhD, P. W., MSc, C. W., PhD, N. I., MMath, G. C.-D., MPH, H. T., PhD, P. G. T. W., PhD, H. F., MRes, A. D., PhD, J. T. G., PhD, M. B., PhD, S. B., MD, A. B., PhD, A. C., PhD, Z. C., PhD, R. F., PhD, K. G., MSc, W. G., MSc, A. H., PhD, W. H., PhD, D. L., PhD, G. N.-G., DPhil, P. S. R., van Elsland PhD, S., PhD, E. V., MSc, H. W., Wang, Y., MSc, X. X., ScD, P. C. A. D., PhD, P. A. C. G., and DPhil, P. N. M. F. (2020). "Estimates of the severity of coronavirus disease 2019: a model-based analysis". *The Lancet Infectious Diseases*, pages 1–9.

[11] Prem, K., Liu, Y., Russell, T. W., Kucharski, A. J., Eggo, R. M., Davies, N., Flasche, S., Clifford, S., Pearson, C. A., Munday, J. D., et al. (2020). "The effect of control strategies to reduce social mixing on outcomes of the covid-19 epidemic in wuhan, china: a modelling study". *The Lancet Public Health*, 5(5):e261–e270.

[12] Rohith, G. and Devika, K. (2020). "Dynamics and control of covid-19 pandemic with nonlinear incidence rates". *Nonlinear Dynamics*, 101(3):2013–2026.

[13] Shinde, G. R., Kalamkar, A. B., Mahalle, P. N., Dey, N., Chaki, J., and Hassanien, A. E. (2020). "Forecasting models for coronavirus disease (covid-19): a survey of the state-of-the-art". *SN Computer Science*, 1(4):1–15.

[14] Sun, Q. and Min, L. (2014). "Dynamics analysis and simulation of a modified hiv infection model with a saturated infection rate". *Computational and mathematical methods in medicine*, 2014.

[15] Takeuchi, Y., Ma, W., and Beretta, E. (2000). "Global asymptotic properties of a delay sir epidemic model with finite incubation times". *Nonlinear Analysis: Theory, Methods & Applications*, 42(6):931–947.